Robotization of the IR-Thermographic technique – impact on the visualisation quality and considerations on the data workflow

IOP Conf. Series: Materials Science and Engineering 1306 (2024) 012035 doi:10.1088/1757-899X/1306/1/012035

Robotization of the IR-Thermographic technique – impact on the visualisation quality and considerations on the data workflow

N Montinaro [1], C Mineo [2], A Pantano [1] and D Cerniglia [1]

[1] Department of Engineering, University of Palermo, 90128 Palermo, Italy;

[2] Institute for High-Performance Computing and Networking, National Research Council of Italy, 90146 Palermo, Italy

Corresponding author email: nicola.montinaro@unipa.it

Abstract. Quality control automation is becoming increasingly popular in industrial production lines. Active thermography techniques are well-regarded for their adaptability, providing fast, non-contact, and full-field non-destructive evaluation. Automating thermographic evaluation can increase assessment speed and repeatability without sacrificing inspection accuracy. By using a robot arm to manipulate the thermographic setup, it becomes possible to inspect large components and refine scans on suspicious zones, even in parts with complex geometries. In this study, the performance of a new thermographic inspection platform is compared with a conventional setup to showcase the potential improvements. A plastic curved-shaped sample with artificial flat bottom hole defects is used as a benchmark for the comparison. The advantages and disadvantages of robotizing the infrared non-destructive setup are analyzed, and the impact of the data workflow and future research activities are also discussed.

1. Introduction

Non-destructive tests (NDTs) are the sum of examinations, tests, and surveys accomplished through methods that do not alter the material and do not require the destruction or removal of samples from the structure, aimed at detecting and characterizing flaws. This type of test makes it possible to assess the damage in the examined object without compromising its continued usability [1].

Conventional manual NDT techniques are insufficient in some scenarios since they could cause a manufacturing process bottleneck, and call for skilled experts [2]. Consequently, there exist underlying incentives for augmenting automation in nondestructive testing. These days, it is possible to quickly produce large and complicated geometries by combining cutting-edge additive manufacturing techniques with conventional subtractive methods thanks to computer-aided design (CAD) and computer-aided manufacturing (CAM) [3]. As a result, NDT automation will need to handle the examination of these complex structures. Although manual scanning remains suitable for specific areas of a structure, the industry emphasizes creating reliable automated solutions to cut down on inspection times and costs. An industrial robot is a versatile manipulator that can be autonomously operated and programmed in three or more axes [4]. Some modern robot solutions fall within the range of robot manipulators that are appropriate for creating automated NDT systems. They offer precision mechanics,

the ability to master every joint precisely, and the capacity to output positional data at rapid update rates. The following are the primary challenges in implementing a robotic NDT system:

- coupling the robotic manipulator with the NDT instrumentation;
- developing an NDT software for data collection and visualization;
- developing an appropriate robot inspection route for the component under inspection.

To get over these challenges, some six-axis robotic arm applications for automating ultrasonic nondestructive testing (NDT) inspection have been developed [5–11]. Other than these uses, automation has not been attained in other inspection kinds; thermographic infrared (IR) testing is one example of this. Infrared thermography is a non-destructive method used to obtain and visualize thermal images. In active infrared thermography, an IR camera is used to track the surface temperature's temporal evolution while a heat flow is applied to the component being tested. The idea behind defect identification is that various materials possess distinct thermo-physical characteristics, which result in unique thermal signatures that an infrared sensor, like an IR camera, can detect [12–14]. Even though a thermographic setup in reflection mode, with a heat excitation source and an IR camera on the same side of the part under inspection, is not ideal for detecting deep defects, it offers some advantages over ultrasonic-based inspections. Infrared thermography (IR-NDT) is a contactless and full-field technique. It allows for the remote inspection of the entire area of a component within the field of view of an IR camera at once. Over the last few decades, IR-NDT techniques have become widely popular due to the availability of accurate and affordable devices in the market. The primary benefit of robotizing IR thermography is the ability to inspect large, intricately shaped components by capturing multiple thermographic images from specific positions. Additionally, critical parameters for defect detection, including spatial resolution, energetic resolution, thermal energy input, and sampling rate, can be selected without any trade-offs and with greater flexibility.

Initial research on active thermography examination employing industrial robots as manipulators can be found in [15–16]. Detecting and characterizing flaws requires accurate and consistent pixel blending, which makes thermographic picture alignment difficult for NDT examination. Due to incorrect alignment and blending, the composite thermography image may contain erroneous artifacts, which could result in a false-positive defect diagnosis. The authors of [17] tackled the problems of thermographic picture fusion by creating a process for automatically transforming, aligning, and blending thermographic acquisition data. This work demonstrates the improvements that can be achieved with the new robotized IR-thermographic inspection platform. Investigating artificial flat bottom hole flaws on a curved plastic sample allows for a comparison. The benefits and drawbacks of automating the IR-NDT setup are examined, followed by a discussion of the data workflow's impact and next research projects.

2. IR-thermography

Infrared thermography is a non-contact optical imaging technique used to detect infrared radiation. In the field of non-destructive testing (NDT), it is used to assess the structure, monitor the distribution of infrared radiation, and convert the measurements into a temperature scale. The two primary categories of the IR-NDT are often classified as passive and active. In passive ones, anomalies in the temperature distribution point to areas of concern. This method has important applications in several domains, including manufacturing processes, predictive maintenance, medicine, and building thermal efficiency assessment programs. It is mostly utilized for qualitative inspection to identify anomalies.

Active thermography was developed to lessen the susceptibility to environmental factors and produce more accurate findings. In active thermography, a thermal contrast is created in the thermographic image of the part's surface by an external heat source. Since an object with internal anomalies (such as voids, delamination, or inclusions) will need to be excited into a thermal disequilibrium to produce a characteristic thermal signature that can be detected with an IR camera, the latter method is especially well-suited to nondestructive testing (NDT). Various methods have been created based on the kind of

external stimuli that are being used. Pulsed (PT), step heating (SHT), and lock-in (LIT) are the most often used thermal stimulation techniques. In Figure 1 a schematic representation of the PT and SHT is shown. In [18] a detailed comparison of the LIT and PT approach are compared to quantitatively characterize artificial flaws in steel and carbon fiber-reinforced plastic. With the same aim to quantitatively characterize flaws in composite material, the quadrupole method is used in [19] in comparison to the PT and thermal signal reconstruction method (TSR).

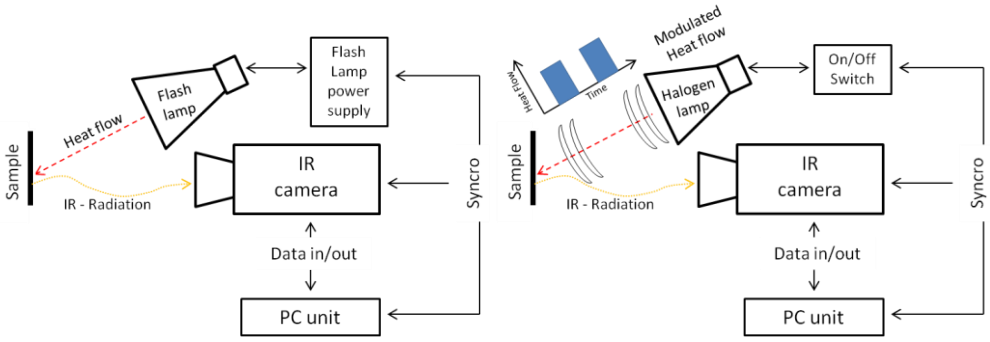

Figure 1. Schematic representation of the traditional active IR thermographic setup for pulsed thermography (on the left) and step heating (on the right).

The geometry, material, and size of the flaw of the being inspected part usually determine the best approach and configuration to be used. Research has indicated that not all defects can be easily identified using the same method; for instance, not all materials react noticeably to the same heating source [20]. PT is the most promising method for robotization because of its simplicity and speed. An alternative IR-thermographic system that holds potential for robotization utilizes a small laser for heat injection instead of a bulkier flash lamp. The use of laser excitations to detect vertical cracks in metal parts and delamination/debonding in composite materials has been experimentally applied in [21–23]. The active IR techniques are also profitably used to inspect the typical flaws in metal additively manufactured parts [24-25].

To minimize environmental effects and enhance the thermal contrast of the defect, PT data is often post-processed. In pulsed phase thermography (PPT), the phase and frequency of the PT acquisitions are extracted through post-processing employing the same principles used in lock-in thermography [14, 26–28]. In particular, flashlights emit quick and high-intensity bursts of heat while the following temperature decline is recorded by the IR camera over a truncation window. Once the raw data has been collected, the Discrete Fourier Transform (DFT) is calculated to find the frequency content of the temperature response. Lastly, the phase of a certain harmonic content can be extracted and shown as a phasegram. The value assigned to each pixel in the image represents the phase of the object. Any sudden change in phase indicates a potential issue or is a result of the object's shape. In the PPT method, deeper anomalies are more clearly visible in the low-frequency phasegrams, while the high-frequency phasegram is better suited for sub-cortical flaws. It is also expected that normalizing the signal when assessing the phase will reduce the negative effects of uneven heat distribution and ambient reflections.

3. Methods

3.1. Data workflow

The robotization of the IR-NDT technique enables precise adjustment of critical inspection parameters (e.g., integration time, sample rate, focal distance) without the typical trade-offs of the conventional technique. This enhanced flexibility leads to improved defect detection and characterization performance on samples of various shapes and materials.

The key parameters to be configured in a PT inspection setup are summarized in Table 1. Figure 2 illustrates the data workflow of the proposed robotized inspection method. The data workflow of the robotized inspection platform begins with defining the input parameters. These parameters are selected based on the anticipated defect type, its shape, and position. Typically, an expert adjusts the IR camera acquisition parameters and the experimental setup geometry to define these critical settings.

Table 1. Main parameters to be set in the IR-thermography robotized setup.

Feature	Physical phenomena involved	Parameter to set
Part material	Thermal wave velocity	Length of acquisition, sample rate (frame per second)
Position of the defect concerning the scanned surface	Thermal wave travel distance	Length of acquisition, integration time
Planar dimension of the defect	Field of view	Spatial resolution, focal distance, lens
Type of defect/inclusion	Wave scattering	Integration time, sample rate (frame per second)
Size of the part	Field of view	Number of poses, scanning path

After defining the input parameters, they are inserted into the offline programming user interface (2) created in MATLAB (refer to [17] for more information). The graphical user interface enables the creation of a raster inspection tool path for the sample, based on the user-specified maximum spacing between consecutive image acquisition poses and offset from the sample edges.

After obtaining the IR videos (one for each pose), the data needs to undergo post-processing for accurate visualization and interpretation. After completing step 3 in Figure 2, the data can follow either the 4A or the 4B workflow direction. The acquired data, which consists of thermographic temperature map evolutions, is processed individually using a PPT algorithm or any alternative method. Subsequently, the data is aligned and corrected in step 5A using the Fine Pixel-based Alignment Method (FiPAM), the details of which can be found in [17]. Alternatively, the acquired temperature map evolutions for each pose can be merged with the FiPAM and then post-processed with a thermographic algorithm such as the PPT. In both cases, the final outcome is a map of the scanned sample surface in step 6, where the defect signature can be easily detected and eventually geometrically characterized.

3.2 Thermographic images fusion

In order to collect data optimally during automated inspections, significant effort is made to ensure that the robot's tool path is accurately aligned with the sample reference frame [29]. Despite these efforts, there will always be a difference between the actual tool path and the ideal one due to several factors:

- Physical tolerances in the robot joints
- Geometric deviations in the mounting support of the sensing instrumentation
- Residual inaccuracies in the calibration of the part's position
- Discrepancies between the actual sample geometry and the digital model of the part.

The resulting data often shows imperfect alignment when encoded through robot positional feedback and plotted on a single map. This issue leads to a clear misalignment of thermographic images in robotic thermographic inspections. In a practical solution presented in [17], each picture's plotting position and potential aberrations are corrected to provide a misalignment-free full-field view of the sample being examined. This method is suitable when the rough position of the camera (the shooting pose of each image) is known. The direct method finds the best alignment between a pair of images through an iterative search, where one image is transformed in relation to the other using one of the five planar transformations (see Figure 3).

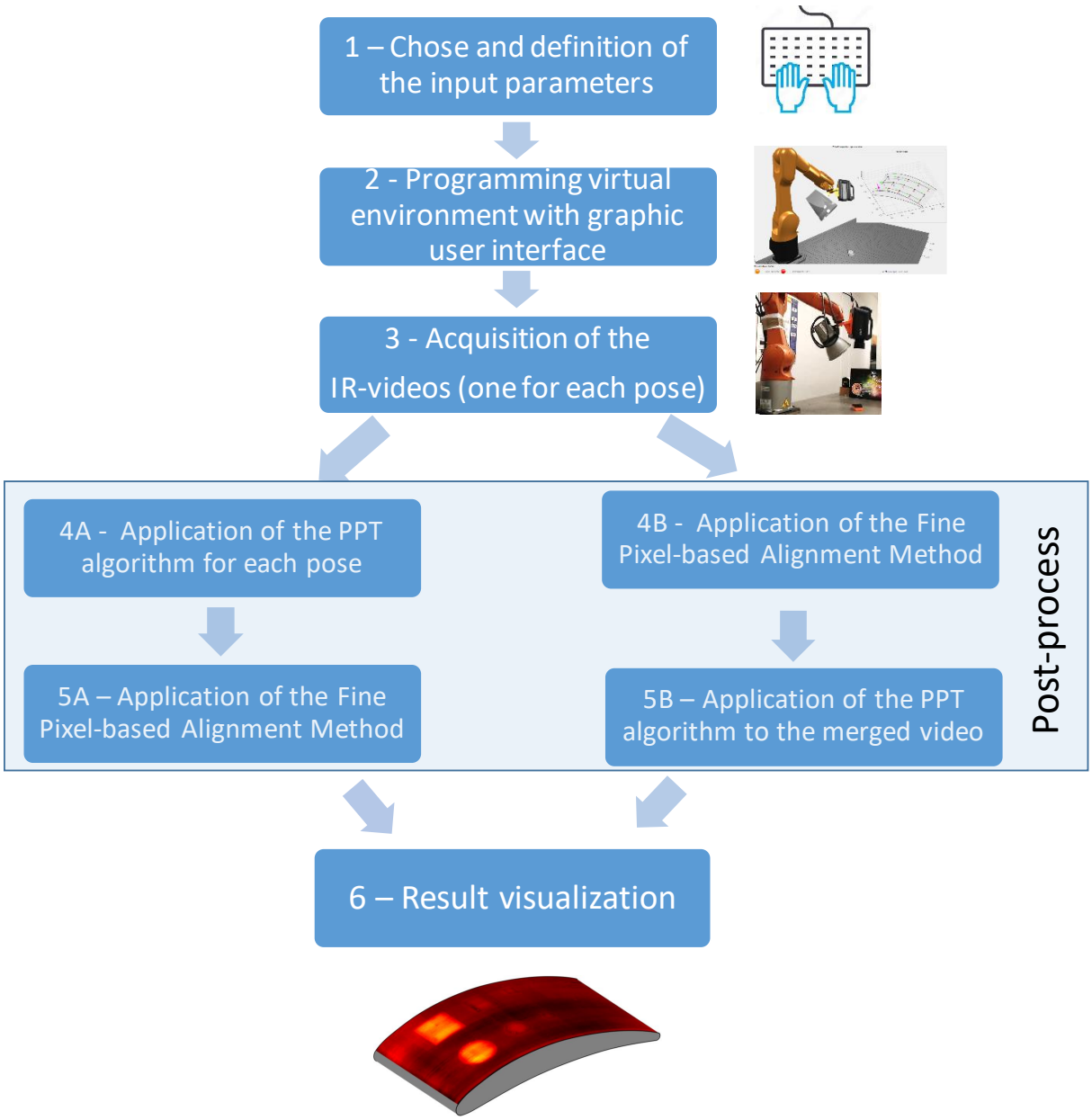

Figure 2. Robotised IR-thermography data workflow.

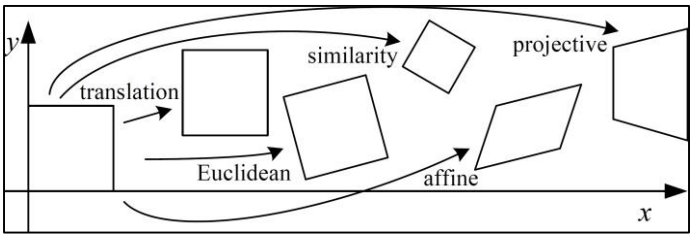

Figure 3. The basic set of 2D planar transformations (source: [30]).

Simply aligning all images in a dataset is not enough to merge them into a single composite image. There may be noticeable variations in pixel brightness across numerous aligned photos where they overlap. To address this, a technique has been developed to preserve the NDT data. The final composite image is created using Laplacian pyramid blending, which allows for a smooth transition between pictures without causing any visual artifacts.

4. Experimental activity

4.1. Sample

The benchmark sample is a piece of bulk epoxy that replicates the curved geometry of a compressor blade with variable thickness. It has one convex side and one concave side, both with a single direction of curvature. On the concave side of the sample, six flat bottom holes (FBHs) were machined as artificial flaws - three with square portions and three with circular sections. As a result, the FBHs are not visible from the sample's convex side. The sample's shape, primary dimensions, and the location and size of the FBHs are shown in Figures 4a and 4b. Additionally, the sample is painted with an acrylic-based, high-temperature resistant matte black paint to enhance the surface emissivity uniformly.

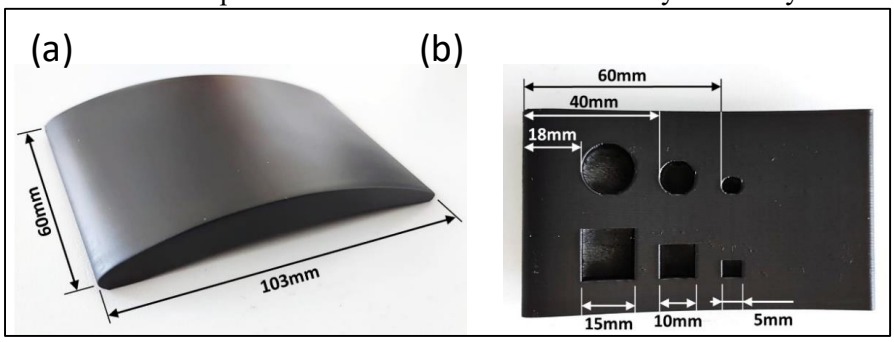

Figure 4. (a) a picture of the curved sample with the indication of its dimensions; (b) a picture of the back side of the sample showing the artificial FBHs location and size;

4.2. Setups

The thermography platform used in this study is illustrated in Figure 5a. The robotic manipulator could carry up to 11.1 kg and had a maximum reach of 110 cm (KUKA KR10 R1100-2 arm [31]). Both the flashlight and the IR camera were positioned on the same side of the component being inspected, as this setup was designed for PT examination in reflection mode. The IR camera and flash lamp were attached to the robot using a custom-made mounting bracket, maintaining a fixed relative position throughout the examination. The support allows for adjusting the orientation of the flash lamp, which enables modification of the angle between the camera axis and the flash lamp's illumination axis. An Elinchrom Twin X4 Lamphead emitting a pulse with a power output of 4800 W/s and a duration of 1/180 s served as a heat source [32]. The adopted IR camera is a cooled FLIR X6540sc equipped with a 640 x 512 (horizontal x vertical) pixel detector [33] and a 50 mm F/2.0 lens. The camera is connected to the PC with a Gigabit Ethernet link for full-bandwidth data acquisition. The MATLAB graphic user interface was used to create a tool path for inspecting a sample. For this particular application a spacing of 25 mm between consecutive poses and a 10 mm offset from the sample edges was set. The inspection path consisted of 15 poses distributed across three passes with five poses each. The Interfacing Toolbox for Robotic Arms (ITRA) [34] was used to control the connection between the computer and the robot.

To evaluate the results obtained by the robotized setup, the same sample has been inspected with a conventional PT experimental setup shown in Figure 4b. The traditional PT setup used the same IR camera and flash lamp as the robotized setup. However, in the robotized setup, the acquisition is sub-windowed to 10% of the full frame while maintaining equal data flow. This allows for a potential increase in sample rate of up to 5.5 times. It's important to note that the focal distance and lens are consistent across both setups. The experimental parameters for both setups are summarized in Table 2.

Table 2. Experimental setup parameters.

	Robotised	**Conventional**
Int. time	3192 µs	3192 µs
Frame per second	100 Hz	18 Hz
Length acquisition	10 s	10 s
Field of view H x V	224 x 192 pixel	640 x 512 pixel
Focal distance	55 cm	55 cm
Type of post-process	PPT	PPT
Resolution	150 µm/pixel.	150 µm/pixel.

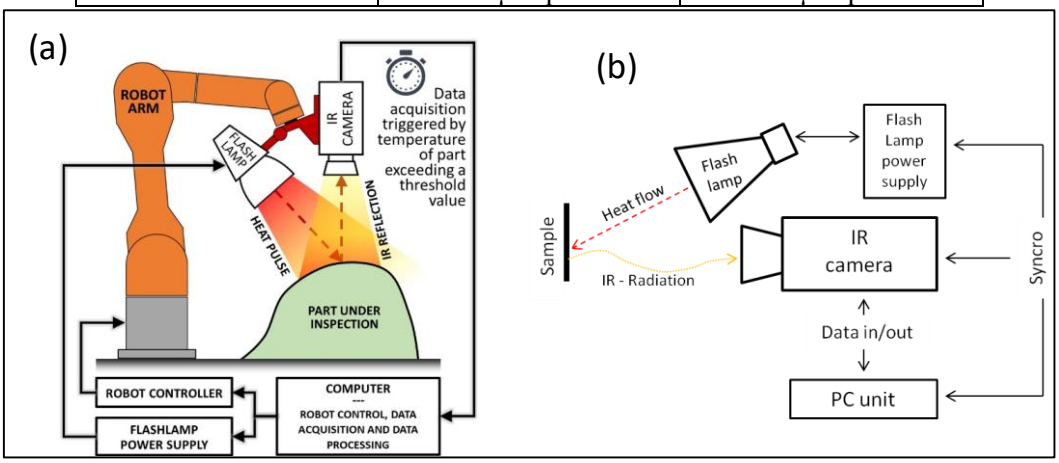

Figure 5. (a) schematic reppresentation of the robotic PT setup; (b) schematic representation of the conventional PT setup used as a comparison.

5. Results and discussion

To assess the platform's performance, we examined the benchmark sample using the same instruments as the traditional PT setup (see Figure 5b) and the robotized setup (see Figure 5a). In both cases, we analyzed the surface temperature's temporal evolution with the PPT algorithm in mind. The data workflow path through 4A and 5A (see Figure 2) is used for this comparison. Figure 6 displays the phasegrams at 0.05 Hz obtained by the PPT algorithm after step 4A of the workflow in Figure 2, but before the FiPAM application 5A. As shown in Figure 6, the original 15 images encoded through the robot poses need alignment and contrast equalization.

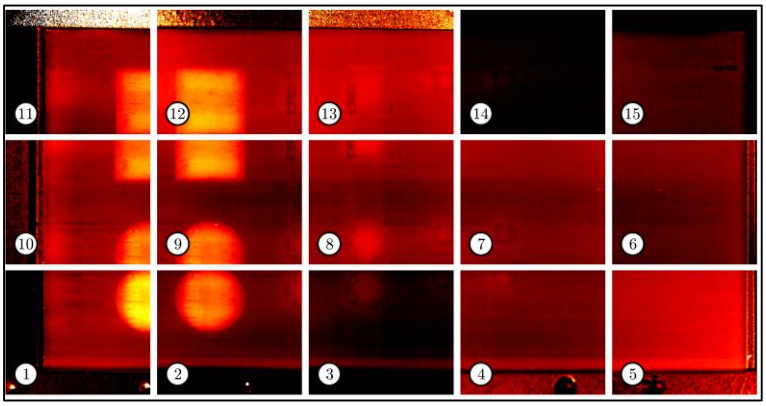

Figure 6. Set of 15 phasegrams at 0.05 Hz before the application of the FiPAM algorithm.

In Figure 7a, the visualization of the composite phasegram obtained after the application of the FiPAM is shown. The similarity transformation, which allows four degrees of freedom (horizontal translation, vertical translation, rotation, and scaling), is proved to be sufficient to permit a fine alignment of the 15 images of the set. In Figure 7b, the post-processed phasegram extracted at 0.25 Hz with the PPT algorithm resulting from the conventional setup is compared.

In Figure 8, the same phasegram of Figure 7a is wrapped onto the CAD model sample surface to increase the clarity of the visualization to a potential NDT operator.

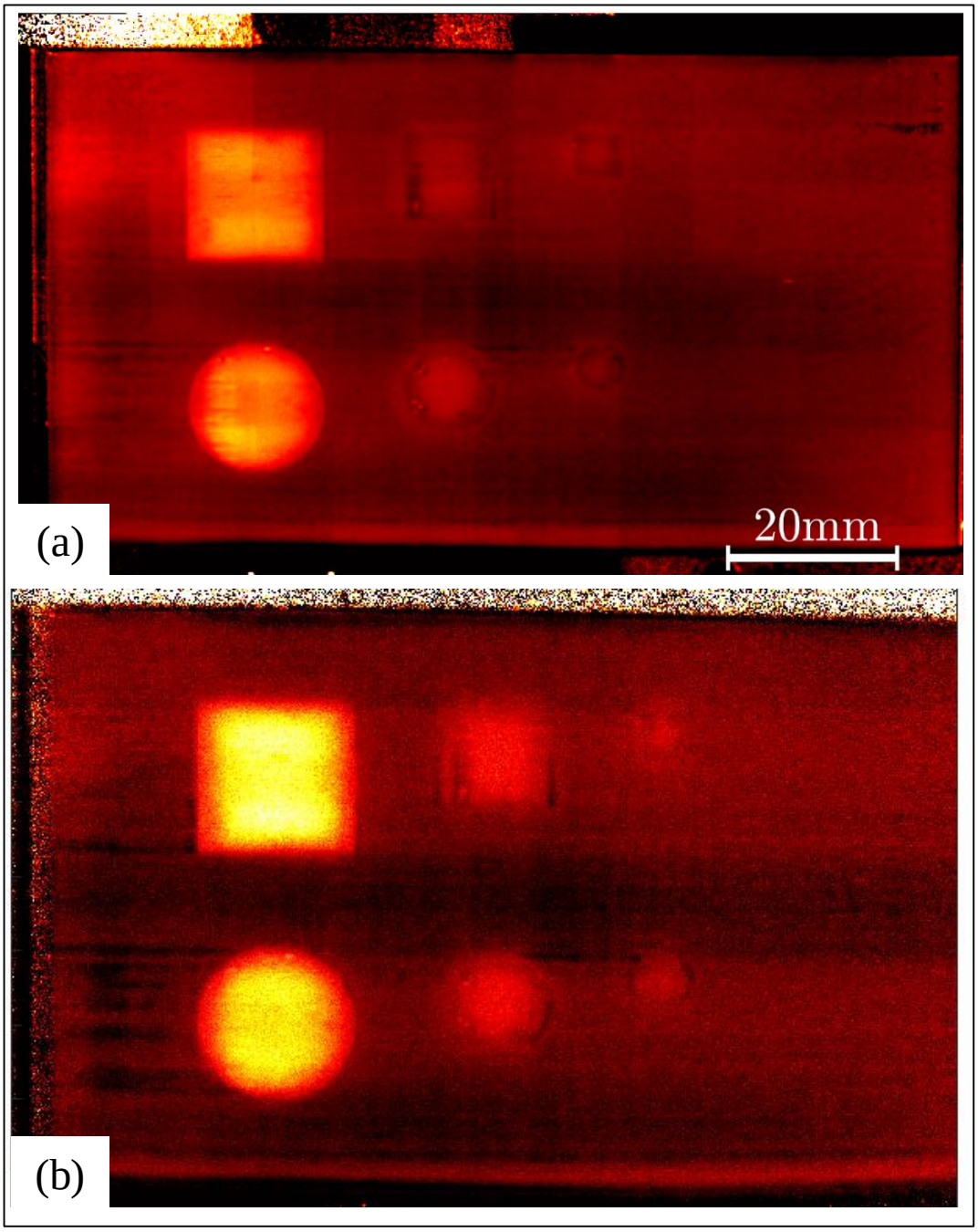

Figure 7. (a) composite phasegram obtained with the robotized setup; (b) phasegram obtained with the conventional setup and same instrumentation.

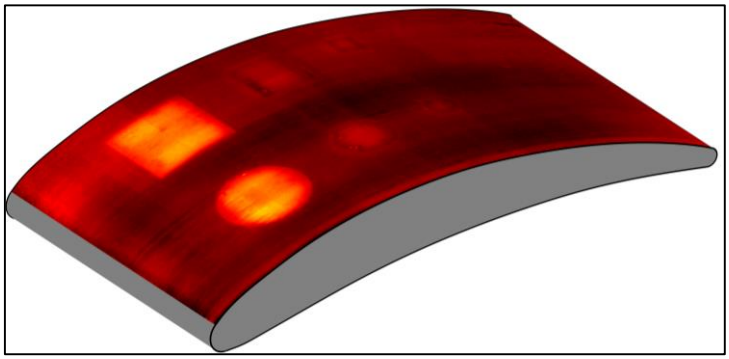

Figure 8. Phasegram of Figure 7a wrapped onto the CAD model of the sample.

The comparison shown on Figure 7 between the two experimental setups shows a clear improvement in the fidelity of reproduction of the position and geometry of the defect. The increased fidelity becomes clearer in the case of smaller defects (both circular or squared). The phasegram coming from the conventional setup with the same PPT algorithm post-process does not allow any geometry characterization but only detection of the defect. Contrariwise, all defects' sizes and positions are faithfully reproduced using the dataset acquired through the robotic platform.

Conventional setup image is then suffering from blurring. This issue is probably due to the fact that only a focal plane can be clearly in focus on the inspection of curved surfaces, thus resulting in a trade-off set. Instead, the robotized inspection allows for reducing the focalization problem, partitioning the whole image, and maintaining the focus in a specific tolerance range. The focalization error decreases with the number of partitions tending to infinity.

The application of the robotic setup does not bring only advantages; in fact, it must be considered that the scanning time for the given area increases linearly with the number of poses into which it is partitioned. Furthermore, the image processing time due to the FiPAM algorithm must be considered. In [17], the computational time for applying the FiPAM was studied.

It must be noted that the presented comparison is performed following the data workflow 4A → 5A (see Figure 2) but different scenarios could be expected in the case of 4B → 5B workflow. In this latter workflow, the temporal evolution of the temperature acquired in the *n* poses will be aligned and merged in a single file and subsequently processed using a PPT algorithm (or another one). This alternative approach would reduce the number of pixels to be processed with the PPT algorithm (which is the most computationally expensive) since the overlapping portions of images are processed only once. The analysis in terms of computational cost and quality of this approach's results will be studied soon. Moreover, future work will investigate on the optimization of the processing algorithms allowing to control the inspection in real time. A data-driven control of the platform would increase the capability of the system to adapt to the part geometry and material acquiring high-quality thermographic data.

References

[1] Hull, JB, Vernon J 2012 Non-Destructive Testing *Springer Nature*
[2] Sattar, TP 2010 Robotic Non-Destructive Testing *Industrial Robot: An International Journal* **37**(5)
[3] Gibson I, Rosen DW, Stucker B, Khorasani M 2021 Additive Manufacturing Technologies *Springer*
[4] Appleton E, Williams DJ 2012 Industrial Robot Applications *Springer Science & Business Media*
[5] Mineo C, Pierce SG, Wright B, Cooper I, Nicholson PI 2015 Paut Inspection of Complex-Shaped Composite Materials through Six Dofs Robotic Manipulators *Insight-Non-Destructive Testing and Condition Monitoring* **57** 3 161-66
[6] Mineo C, Pierce SG, Nicholson PI, Cooper I 2016 Robotic Path Planning for Non-Destructive

Testing–a Custom Matlab Toolbox Approach *Robotics and Computer-Integrated Manufacturing* **37** 1-12
[7] Mineo C, Cerniglia D, Ricotta V, Reitinger B 2021 Autonomous 3D geometry reconstruction through robot-manipulated optical sensors *International Journal of Advanced Manufacturing Technology* **116** (5-6) 1895-1911
[8] Mineo C, Cerniglia D 2023 Adding Autonomy to Robotic Enabled Sensing *Lecture Notes in Civil Engineering* **270** LNCE 338 - 347
[9] Bosse J, Thaler B, Ilse D, Bühling L Automated Air-Coupled Ultrasonic Technique for the Inspection of the Ec145 Tail Boom *NDT in Aerospace 2012* - Tu.2.B.3
[10] Cooper I, Nicholson I, Yan D, Wright B, Liaptsis D, Mineo C 2013 Development of a Fast Inspection System for Aerospace Composite Materials-the Intacom Project *5th International Symposium on NDT in Aerospace 2013-11-13 - 2013-11-15*
[11] Mineo C, Cerniglia D, Poole A 2022 Autonomous Robotic Sensing for Simultaneous Geometric and Volumetric Inspection of Free-Form Parts *Journal of Intelligent and Robotic Systems: Theory and Applications* **105** (3) 54
[12] Meola C 2012 Infrared Thermography Recent Advances and Future Trends Bentham Science Publishers
[13] Holst GC 2000 Common Sense Approach to Thermal Imaging Vol. 1 SPIE Optical Engineering Press Washington
[14] Maldague X 2001 Theory and Practice of Infrared Technology for Nondestructive Testing John Wiley & Sons Inc
[15] Schmidt T, Dutta S 2012 Automation in Production Integrated Ndt Using Thermography *NDT in Aerospace, Augsburg* **8**
[16] Massaro A, Galiano A 2020 Infrared Thermography for Intelligent Robotic Systems in Research Industry Inspections: Thermography in Industry Processes *Handbook of Research on Advanced Mechatronic Systems and Intelligent Robotics*, 98-125 IGI Global
[17] Mineo C, Montinaro N, Fustaino M, Pantano A, Cerniglia D 2022 Fine Alignment of Thermographic Images for Robotic Inspection of Parts with Complex Geometries *Sensors* **22** (16) 6267
[18] Maierhofer C, Röllig M, Krankenhagen R, & Myrach P 2016 Comparison of quantitative defect characterization using pulse-phase and lock-in thermography *Applied optics* **55**(34).
[19] Müller J P, Dell'Avvocato G, & Krankenhagen R 2020 Assessing overload-induced delaminations in glass fiber reinforced polymers by its geometry and thermal resistance. *NDT & E International* **116** 102309
[20] Shull PJ 2002 Nondestructive Evaluation: theory, techniques, and applications New York: Marcel Dekker Ed
[21] Montinaro N, Cerniglia D, Pitarresi G 2017 Flying Laser Spot Thermography technique for the NDE of Fibre Metal Laminates disbonds *Composite Structures* **171** 63–76
[22] Montinaro N, Cerniglia D, Pitarresi G 2018 Evaluation of interlaminar delaminations in titanium-graphite fibre metal laminates by infrared NDT techniques *NDT and E International*, **98** 134–146
[23] Montinaro N, Cerniglia D, Pitarresi G 2019 Evaluation of Vertical Fatigue Cracks by Means of Flying Laser Thermography *Journal of Nondestructive Evaluation*, **38**(2)
[24] D'Accardi E, Krankenhagen R, Ulbricht A, Pelkner M, Pohl R, Palumbo D, & Galietti U 2022 Capability to detect and localize typical defects of laser powder bed fusion (L-PBF) process: An experimental investigation with different non-destructive techniques. *Progress in Additive Manufacturing* **7**(6), 1239-1256
[25] Montinaro N, Cerniglia D, Pitarresi G 2018 A numerical and experimental study through laser thermography for defect detection on metal additive manufactured parts *Frattura ed Integrità Strutturale* **12** (43) 231-240
[26] Maldague X, Marinetti S. 1996 Pulse Phase Infrared Thermography *Journal of applied physics*

79(5) 2694-98
[27] Maldague X, Galmiche F, Ziadi A 2002 Advances in Pulsed Phase Thermography *Infrared physics & technology* **43**(3-5) 175-81
[28] Ibarra-Castanedo C, Maldague X 2004 Pulsed Phase Thermography Reviewed *Quantitative Infrared Thermography Journal* **1**(1) 47-70
[29] Mineo C, Cerniglia D, Poole A 2022 Autonomous Robotic Sensing for Simultaneous Geometric and Volumetric Inspection of Free-Form Parts *Journal of Intelligent & Robotic Systems* **105**(3) 54
[30] Paragios N, Chen Y, Faugeras OD 2006 *Handbook of Mathematical Models in Computer Vision: Springer Science & Business Media*
[31] KUKA Kr 10 R1100-2. https://www.kuka.com/-/media/kuka-downloads/imported/6b77eecacfe542d3b736af377562ecaa/0000290003_en.pdf?rev=3e82b095d46c4a86b7e195cabdb980cb&hash=A4F0F7D35D9485B612F8BC455B5805E4 (accessed 02/04/2024)
[32] Elinchrom Digital Rx. https://www.elinchrom.com/wp-content/uploads/download-center/73256_digital_rx_manuel--en-de-fr.pdf (accessed 02/04/2024)
[33] FLIR X6540sc http://www.flirmedia.com/MMC/THG/Brochures/RND_088/RND_088_US.pdf (accessed 02/04/2024)
[34] Mineo C et al.. 2020 Enabling Robotic Adaptive Behaviour Capabilities for New Industry 4.0 Automated Quality Inspection Paradigms *Insight-Non-Destructive Testing and Condition Monitoring* **62**(6) 338-44